JMEPEG (2005) 14:203-211
DOI: 10.1361/10599490523346

1059-9495/$19.00

Residual Stress Characterization in Structural Materials by Destructive and Nondestructive Techniques

A.K. Roy, A. Venkatesh, V. Marthandam, S.B. Dronavalli, Douglas Wells, and Ronald Rogge

(Submitted August 9, 2004; in revised form November 24, 2004)

Transmutation of nuclear waste is currently being considered to transform long-lived isotopes to species with relatively short half-lives and reduced radioactivity through capture and decay of minor actinides and fission products. This process is intended for geologic disposal of spent nuclear fuels for shorter durations in the proposed Yucca Mountain repository. The molten lead-bismuth-eutectic will be used as a target and coolant during transmutation, which will be contained in a subsystem vessel made from materials such as austenitic (304L) and martensitic (EP-823 and HT-9) stainless steels. The structural materials used in this vessel will be subjected to welding operations and plastic deformation during fabrication. The resultant residual stresses cannot be totally eliminated even by stress-relief operations. Destructive and nondestructive techniques have been used to evaluate residual stresses in the welded and cold-worked specimens. Results indicate that tensile residual stresses were generated at the fusion line of the welded specimens made from either austenitic or martensitic stainless steel, with reduced stresses away from this region. The magnitude of residual stress in the cold-worked specimens was enhanced at intermediate cold-reduction levels, showing tensile residual stresses in the austenitic material while exhibiting compressive stresses in the martensitic alloys. Comparative analyses of the resultant data obtained by different techniques revealed consistent stress patterns.

Keywords neutron diffraction, positron annihilation spectroscopy, residual stress, ring-core, structural materials, transmutation

1. Introduction

Engineering metallic materials and alloys, when subjected to tensile loading beyond a limiting value, undergo plastic deformation resulting in lattice defects such as voids and dislocations. These imperfections interact with the crystal lattice, producing a higher state of internal stress, also known as residual stress, which can be associated with reduced ductility. Residual stresses are also generated in welded metals due to rapid solidification and the resultant dissimilar metallurgical microstructure between the weld and the base metals. Development of these internal stresses is often influenced by incompatible permanent strain resulting from thermal and mechanical operations associated with plastic deformation and cold work. These types of operations can cause premature failures in metals and alloys unless internal stresses are relieved by thermal treatments, which are commonly known as stress-relief operations.

The nuclear waste destined for the proposed geologic repository at the Yucca Mountain site will consist of spent nuclear fuel (SNF) and high-level radioactive waste (HLW). SNF is the used fuel removed from the nuclear reactors at commercial power plants, research reactors, government facilities, and the nuclear Navy. HLW refers to the radioactive materials associated with weapons production. Transmutation and separation of minor actinides (MA) and fission products (FP) from SNF are currently being considered to reduce the radioactivity associated with them. Transmutation refers to the transformation of SNF and occurs when the nucleus of an atom changes due to natural radioactive decay, nuclear fission, neutron capture, or other related processes.

The molten lead-bismuth-eutectic (LBE) was proposed to be a spallation target producing source neutrons from the incident proton beam and simultaneously acting as a blanket coolant, thus removing the generated heat. The molten LBE will be contained in a structural vessel made of a suitable metallic material, often referred to as the target structural material. Fabrication of this containment vessel will involve normal manufacturing processes such as cold deformation, mechanical forming, and welding of similar and dissimilar materials. A significant amount of residual stress can be developed in the container materials during these manufacturing processes unless they are minimized or eliminated by stress-relief operations. However, annealing at elevated temperatures may not be feasible in view of the possible changes in metallurgical characteristics of these structural materials, producing detrimental effects during the spallation process. It should also be realized that the residual stresses due to radiation during the spallation process and the associated hardening of the structural materials can possibly be significantly reduced due to their exposure at the operating temperature ranging between 420 and 550 °C during the transmutation process.

The destructive ring-core (RC) method has been used to measure residual stresses based on the relieved-strain during the coring operation. Simultaneously, nondestructive techniques including neutron-diffraction (ND), x-ray diffraction

A.K. Roy, A. Venkatesh, V. Marthandam, and **S.B. Dronavalli**, Department of Mechanical Engineering, University of Nevada Las Vegas (UNLV), Las Vegas, NV 89154; **Douglas Wells,** Department of Physics, Idaho State University, Pocatello, ID; and **Ronald Rogge,** National Research Council, Chalk River, Ontario, Canada. Contact e-mail: aroy@unlv.nevada.edu, anandvenkatesh@gmail.com.

(XRD), and positron annihilation spectroscopy (PAS) have also been used to measure residual stresses in austenitic and martensitic stainless steels that were subjected to either cold-deformation or welding operations. The test materials were cold reduced by different percentages of their plate thickness by rolling. In addition, plastic deformation in strips was produced by three-point-bending. Welded specimens consisting of similar structural materials were also evaluated for residual stress measurements. The comprehensive test results are presented in this paper.

2. Experimental

Materials tested in this investigation include austenitic 304L stainless steel (UNS S30403) and martensitic alloys EP-823 and HT-9. Their chemical compositions are shown in Table 1. Experimental heats of all three materials were melted by vacuum-induction-melting. They were subsequently forged and rolled into plate materials of desired dimensions. These materials were then heat treated prior to machining the test specimens. The 304L stainless steel (SS) plates were solution-annealed at 1010 °C (1850 °F) for 1 h followed by air cooling. The EP-823 and HT-9 alloys were austenitized at a similar temperature followed by an oil-quench. The quenched plates were subsequently tempered at 621 °C (1150 °F) followed by air-cooling. This thermal treatment produced a fully tempered martensitic microstructure without any retained austenite. The microstructures of both austenitic and martensitic stainless steels are shown in Fig. 1(a) and (b), respectively. The room-temperature tensile properties of all three alloys in the heat-treated condition are shown in Table 2.

A part of the heat-treated plates was further plastically deformed by cold rolling to reduce the plate thickness by approximately 3%, 7%, and 11%. Some of the heat-treated plates were cut into strips with a smaller width and were subsequently deformed by three-point-bending (TPB) to produce a gradual residual stress gradient along their lengths. These strips were electropolished prior to the bending process to remove the surface cold work and the residual stresses generated during the machining operation. The central portion of the beam was displaced upward by ~38 mm (1.5 in.) due to bending while maintaining a separation distance of ~255 mm (10 in.) between the two ends. Welded specimens consisting of similar alloys on both sides were prepared using the gas-tungsten-arc-welding (GTAW) method. The welding temperature and the temperature at the tip of the arc were 982 and 4000 °C, respectively. For welded specimens consisting of austenitic SS on both sides, 308L SS filler metal was used. However, in the case of the welded specimens consisting of the martensitic alloys, 2283L was used as the filler material. The configurations of all three types of tested specimens are shown in Fig. 2. The resultant residual stresses in these specimens were measured by different techniques including the RC, ND, XRD, and PAS methods.

The RC method is a mechanical/strain gauge technique aimed at determining the principle residual stresses as a function of depth in polycrystalline or amorphous materials. The method used in this study consisted of dissecting the desired location of the test specimen as a 6.35 mm (0.25 in.) diameter

Table 1 Chemical composition of materials tested

Material (heat number)	Composition, wt.%											
	C	Mn	P	S	Si	Cr	Ni	Mo	Cu	W	Al	Fe
304L SS (2239)	0.02	1.63	0.003	0.005	0.40	18.20	9.55	0.03	0.03	…	0.011	Bal.
EP-823 (2154)	0.17	0.54	0.005	0.004	1.11	11.69	0.65	0.73	0.01	0.63	0.023	Bal.
HT-9 (2155)	0.20	0.40	0.011	0.003	0.19	12.50	0.53	0.99	0.01	0.46	0.029	Bal.

Table 2 Room-temperature tensile properties

Material (Heat number)	Thermal treatment	YS, MPa	UTS, MPa	El, %	RA, %
304L SS (2239)	SA	328	499	66.6	51
EP-823 (2154)	Q&T	713	858	24.9	61
HT-9 (2155)	Q&T	798	962	21.4	61

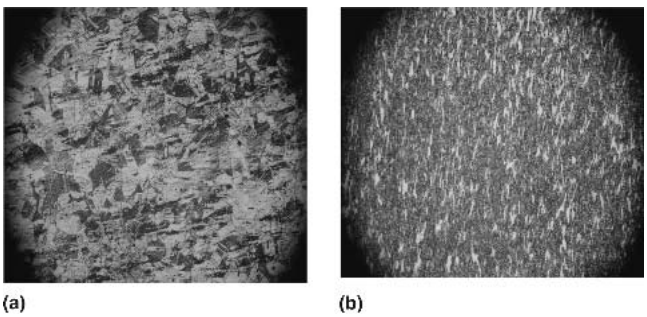

Fig. 1 Microstructure of austenitic and martensitic materials: (a) type 304L SS and (b) alloy EP-823

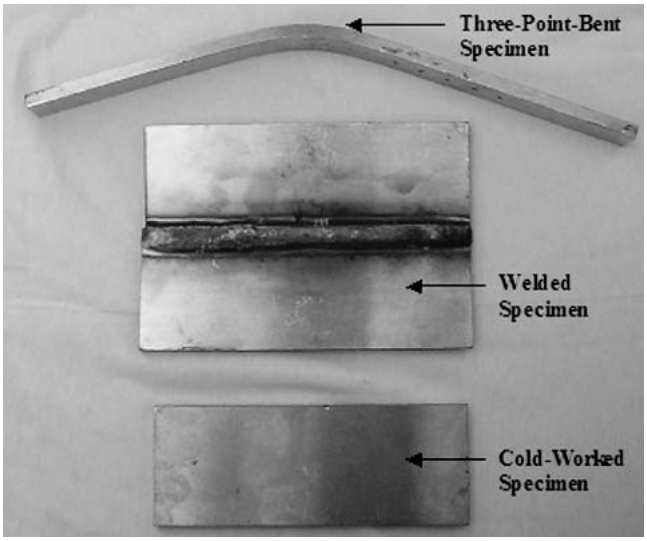

Fig. 2 Types of specimens tested

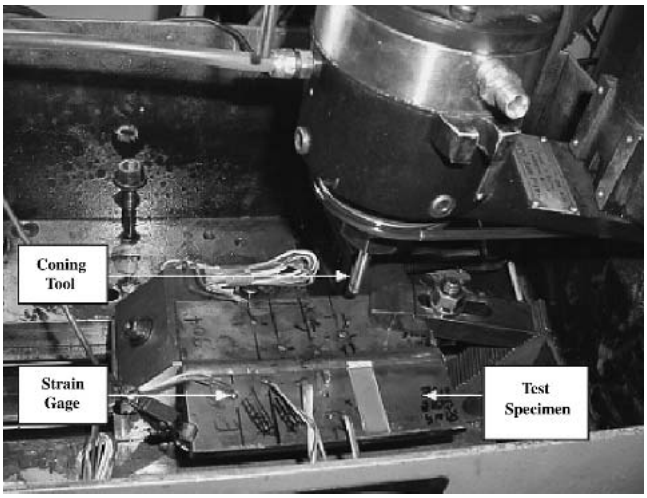

Fig. 3 Experimental setup for ring-core measurements

plug containing the strain gauges, as shown in Fig. 3. The strain, relieved during the coring operation, was measured on the surface of the material remaining inside the ring. The magnitude of residual stress existing in the material before the coring operation was calculated using the measured strain and the appropriate stress-strain relationships (Ref 1).

During the RC method, surface preparation must occur to fix the strain gauges onto the test specimen. Therefore, the surface of the specimen was cleaned with acetone. The strain-gauge rosettes were fixed onto the test specimen with the help of epoxy. Each rosette consisted of three superimposed strain-measuring grids, each angularly displaced by 45°, as shown in Fig. 4. The epoxy was then allowed to cure. Mechanical displacements were applied to the test specimen to ensure proper working of the strain gauges. After setup of the machine, the strain gauges were connected and a zero strain was assigned to it to measure the change in strain, $d\varepsilon$. The total depth of measurement and the depth increments were selected before starting the test. The data acquisition program used the $d\varepsilon$ value and plotted the strain (ε) as a function of the depth (z). This data was then analyzed using a data reduction software that enabled the calculation of $d\varepsilon/dz$. The residual stresses were calculated using the following equations, which are derived using the fundamentals of mechanical metallurgy (Ref 1):

$$\sigma_a(z) = \frac{E}{K_1^2(z) - \nu^2 K_2^2(z)} \left[K_1(z) \frac{d\varepsilon_a(z)}{dz} + \nu K_2(z) \frac{d\varepsilon_c(z)}{dz} \right] \quad \text{(Eq 1)}$$

$$\sigma_b(z) = \frac{E}{K_1^2(z) - \nu^2 K_2^2(z)} \left[K_1(z) \frac{d\varepsilon_b(z)}{dz} + \nu K_2(z) \left(\frac{d\varepsilon_a(z)}{dz} - \frac{d\varepsilon_b(z)}{dz} + \frac{d\varepsilon_c(z)}{dz} \right) \right] \quad \text{(Eq 2)}$$

$$\sigma_c(z) = \frac{E}{K_1^2(z) - \nu^2 K_2^2(z)} \left[K_1(z) \frac{d\varepsilon_c(z)}{dz} + \nu K_2(z) \left(\frac{d\varepsilon_a(z)}{dz} \right) \right] \quad \text{(Eq 3)}$$

where ε_a is the strain measured in direction a, ε_b is the strain measured in direction b, ε_c is the strain measured in direction c, E is Young's modulus, ν is Poisson's ratio of the material

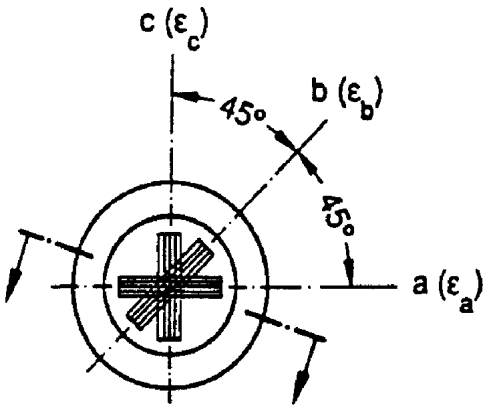

Fig. 4 Strain gauge rosette arrangements

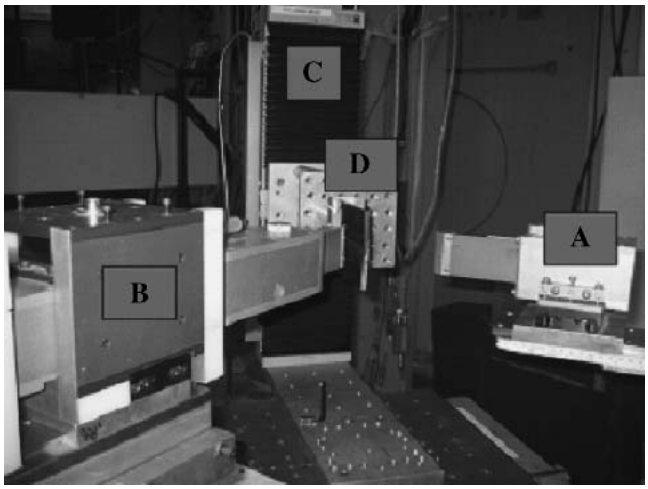

Fig. 5 ND test setup showing (a) incident-beam slit, (b) diffracted-beam slit, (c) X, Y, and Z translators, and (d) the test specimen

under study, σ_a is the residual stress in the material measured by strain gauge a, σ_b is the residual stress in the material measured by strain gauge b, σ_c is the residual stress in the material measured by strain gauge c, and $K_1(z)$ and $K_2(z)$ are relaxation functions in the uniaxial stress state.

The relaxation functions must be known for the RC method to be useful. They were determined by a calibration process in a uniaxial tensile test before the actual ring-core measurements took place. The calibration test was carried out using the same equipment under similar operating conditions as for the residual-stress measurements. The relaxation functions are dependent on the core diameter, the shape of the groove bottom, and the geometrical arrangement of the strain-gauge rosette as well as the residual-stress state and the groove depth.

The ND method relies on elastic deformations within a polycrystalline material that cause changes in the spacing of the lattice planes (d-spacing) from their stress-free value. During this experiment, a collimated neutron beam of known wavelength (0.156 nm) was diffracted by the test specimen, which then passed through a second collimator finally reaching the detector, as illustrated in Fig. 5. The interplanar distance (d) can be evaluated using the Bragg's law, and the corresponding lattice strain can be evaluated using the following equation:

$$\varepsilon_{hkl} = \frac{d_{hkl} - d_0}{d_0} \quad \text{(Eq 4)}$$

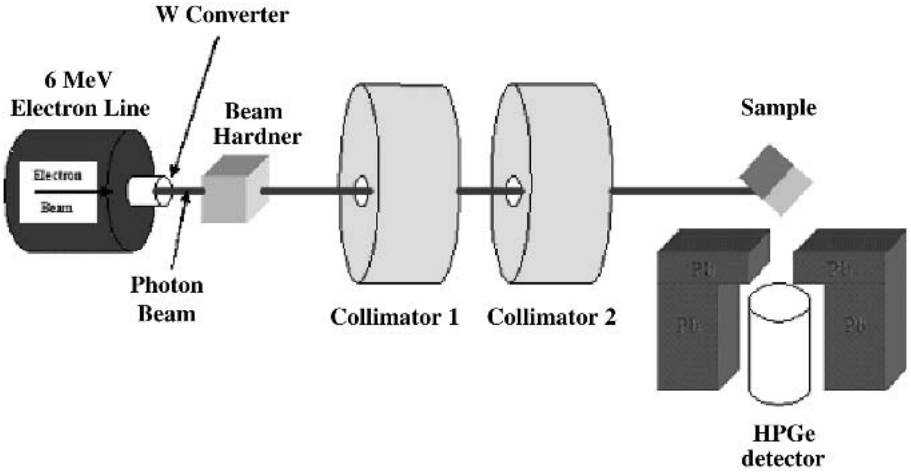

Fig. 6 PAS test setup

where d_{hkl} is the interplanar distance in the stressed material, d_0 is the interplanar distance in a stress-free material, and ε_{hkl} is the lattice strain.

The stress values were subsequently determined from these calculated lattice strains using appropriate mathematical equations (Ref 2). When the diffraction data are taken from many grains of randomly oriented polycrystals, the strains measured by the neutrons correspond to macro-strains and are related to the macro-stresses by the equation of isotropic elasticity. In an elastically-isotropic model, the principal stresses σ_{xx}, σ_{yy}, σ_{zz} are related to the strains by the following equations:

$$\sigma_{xx} = \frac{E}{(1+\nu)(1-2\nu)}[(1-\nu)\varepsilon_{xx} + \nu(\varepsilon_{yy} + \varepsilon_{zz})] \quad \text{(Eq 5)}$$

$$\sigma_{yy} = \frac{E}{(1+\nu)(1-2\nu)}[(1-\nu)\varepsilon_{yy} + \nu(\varepsilon_{xx} + \varepsilon_{zz})] \quad \text{(Eq 6)}$$

$$\sigma_{zz} = \frac{E}{(1+\nu)(1-2\nu)}[(1-\nu)\varepsilon_{zz} + \nu(\varepsilon_{xx} + \varepsilon_{yy})] \quad \text{(Eq 7)}$$

where E is Young's modulus, ν is Poisson's ratio, ε_{xx} is the principal strain in the X-direction, ε_{yy} is the principal strain in the Y-direction, and ε_{zz} is the principal strain in the Z-direction.

Due to the anisotropy of elastic properties in crystalline materials, the values of E and ν at a microscopic level depend on the lattice planes (*hkl*) considered. Thus, the neutron elastic constants must be known or can be determined experimentally (Ref 2). The nature of residual stress (tensile versus compressive) was also evaluated by analyzing the magnitude of the d parameter.

The XRD technique operates on a principle similar to the ND method, the only difference being the depth of beam penetration. Although the XRD method is a well-established technique to measure residual stresses in engineering components, it is usually limited to near-surface measurements (Ref 3-5). The XRD technique is based on the premise that when a metal is under an applied or a residual stress, the resultant elastic strains would cause the atomic planes in the crystal structure to change their d-spacing. The magnitude of the d-spacing enables determination of the residual stresses in the material. A similar principle applies to the residual stress measurements by the ND technique.

PAS is a well-established nondestructive technique that is used to characterize defects in materials (Ref 6). The technique used in this investigation employs high-energy, deep-penetrating γ-rays (6 MeV) into thick samples of the materials of interest to measure stress, strain, and defects in them. A collimated photon beam from a linear accelerator (Linac) was used to generate positrons inside the test specimen via pair (positron/electron) production, as shown in Fig. 6. Each positron generated by this technique was thermalized and annihilated with one of the sample electrons emitting two photons having a 511 keV energy spectrum. These photons were then recorded by a high-energy resolution HPGe (i.e., high-purity Ge) detector, and the resultant data were analyzed in terms of the three line-shape parameters S, W, and T of the 511 keV annihilation peak, as shown in Fig. 7 (Ref 7,8). The S and W parameters have often been used to characterize the annihilation peak in Doppler broadening spectroscopy (Ref 7). The S parameter is sensitive to the annihilation with valence electrons and is defined as the ratio of the counts in the central region of the peak to the total counts in the peak. The W-parameter is more sensitive to the annihilation with high momentum core electrons and is defined as the ratio of the counts in the wing regions of the peak to the total counts in the peak. The T-parameter is simply the ratio of W to S. The residual stresses developed in the test specimens were qualitatively analyzed in terms of these parameters. While the S-parameter is directly proportional to the residual stress, the T-parameter is inversely proportional to the internal stress developed inside the test specimens.

3. Results and Discussion

3.1 RC Measurements

The results of residual stress measurements by the RC method on the cold-worked specimens of austenitic and martensitic materials subjected to three different levels of cold-reduction (CR), are shown in Fig. 8, 9, and 10, respectively. An examination of Fig. 8 indicates that the residual stresses gen-

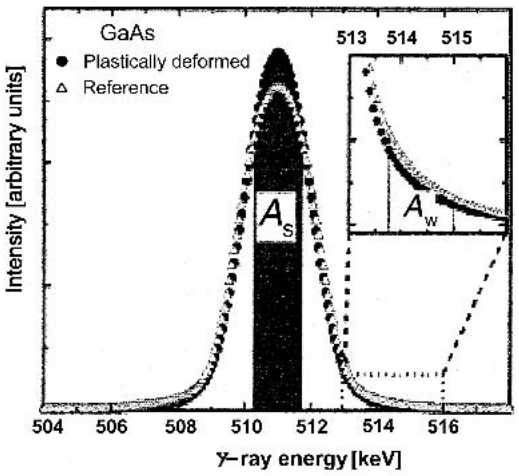

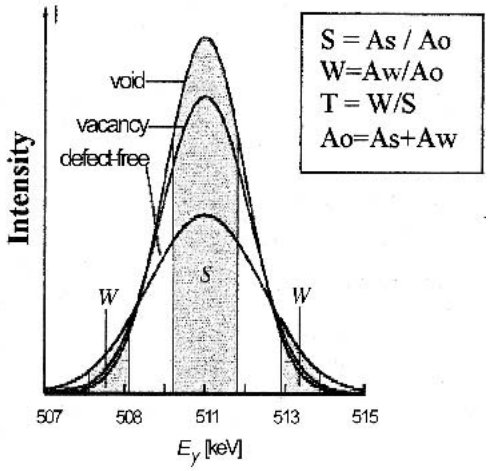

Fig. 7 Characteristics of 511 KeV gamma–ray energy spectrum

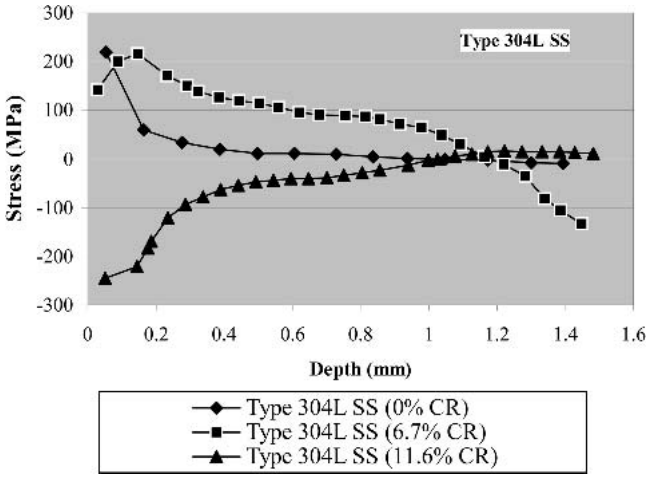

Fig. 8 Residual stresses versus depth profile for 304L SS (RC method)

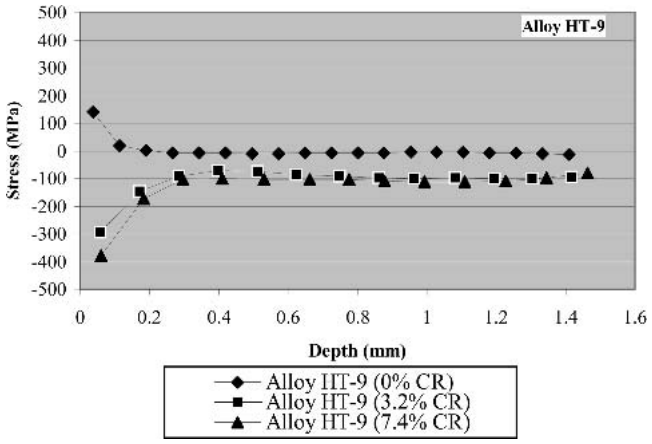

Fig. 9 Residual stress versus depth profile for HT-9 (RC method)

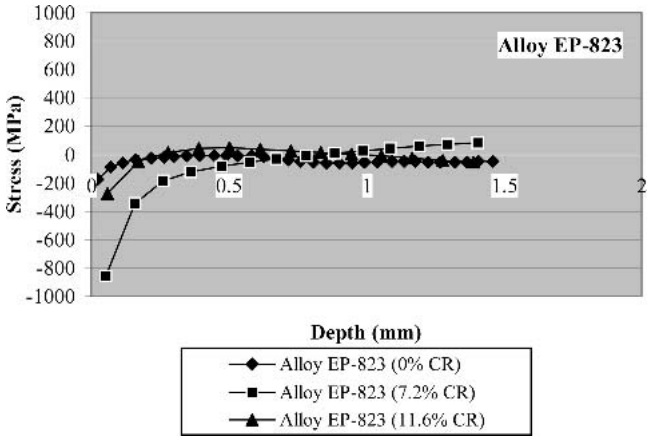

Fig. 10 Residual stress versus depth profile for EP-823 (RC method)

erated in 304L SS due to CR of 6.7% were tensile in nature, gradually becoming compressive at greater depths. As expected, the specimen that did not undergo any CR showed very little or no residual stresses. However, the residual stresses generated due to the increased level (11.6%) of CR were initially compressive, gradually becoming less compressive with increasing depth.

The results of residual stress measurements on the two martensitic alloys, namely HT 9 and EP-823, by the RC technique, as shown in Fig. 9 and 10, reveal a different pattern. For both alloys, the residual stresses generated at CR of 3.2 and 7.2%, respectively, were compressive in nature. However, these stresses became less compressive with increasing depth, approaching a zero-level stress value. Once again, both martensitic alloys without any CR displayed zero stress, as expected. Only a slight variation in residual stresses were observed with these materials due to the increased levels (7.4% and 11.6%, respectively) of CR, as illustrated in Fig. 9 and 10.

The results of residual stress measurements on the welded 304L SS, EP-823 and HT-9 specimens by the RC method are illustrated in Fig. 11, 12 and 13, respectively. An evaluation of the stress pattern shown in these figures consistently demonstrates that the residual stresses were tensile in the vicinity of the fusion line for all three alloys. The extent of the internal stresses was a maximum in this region compared to those developed at distances away from the fusion line, also as expected. It is well known that the maximum residual stress can be generated at the fusion line due to the rapid solidification and dissimilar metallurgical microstructures between the weld and base metals.

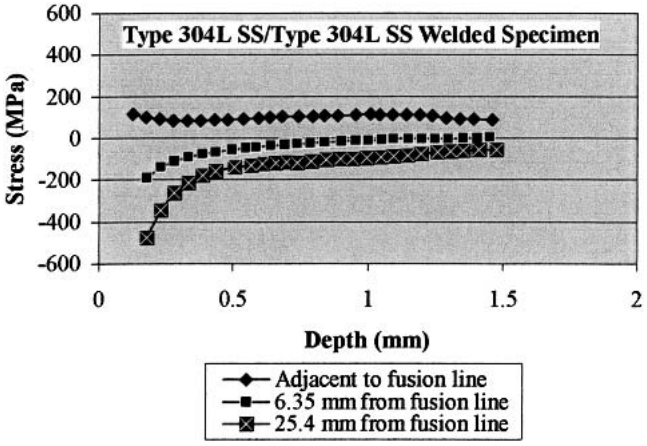

Fig. 11 Residual stress versus depth as a function of distance from fusion line (RC method)

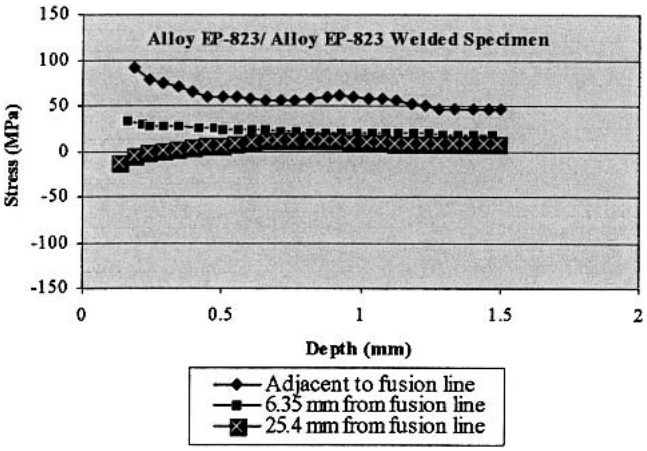

Fig. 12 Residual stress versus depth as a function of distance from fusion line (RC method)

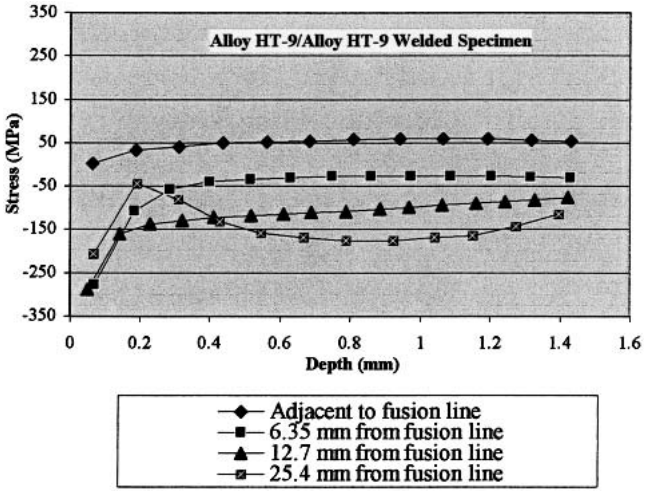

Fig. 13 Residual stress versus depth as a function of distance from fusion line (RC method)

3.2 ND/XRD Measurements

The results of residual stress measurements by the ND technique on an EP-823 specimen subjected to 11.6% CR are

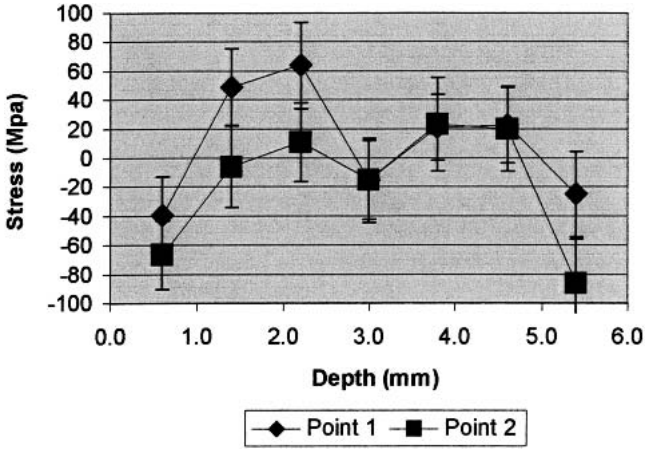

Fig. 14 Residual stress profile for EP-823 with 11.6% CR (ND method)

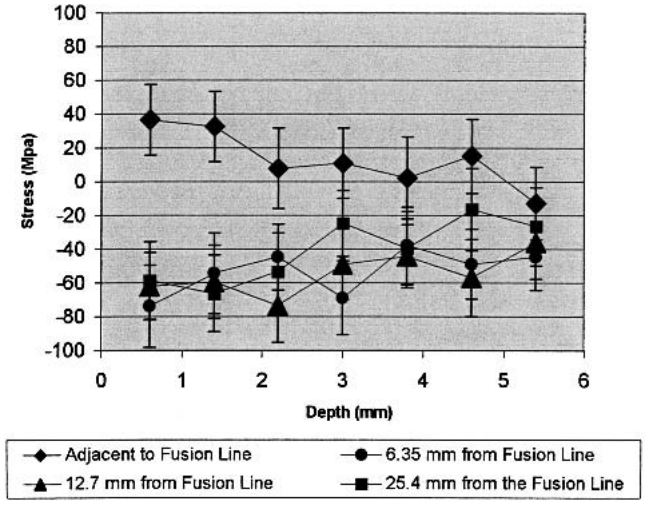

Fig. 15 Residual stress profile for HT-9/HT-9 welded specimen (ND method)

shown in Fig. 14 at two different selected locations along its rolling direction. These data indicate that compressive residual stresses were generated near the surface followed by alternate tensile and compressive stresses at greater depths.

With respect to the stress measurements performed by the ND technique on a welded specimen consisting of HT-9 on each side, tensile residual stresses were observed adjacent to the fusion line followed by a gradual reduction at locations away from the welded region, as anticipated. The resultant data are shown in Fig. 15.

Residual stresses, measured on three-point-bent (TPB) specimens of 304L SS and HT-9 along their thickness by the ND technique, showed a consistent pattern. The data, shown in Fig. 16 and 17, clearly indicate that the stresses developed in both materials at the apex (convex side) of the TPB specimens were compressive compared to the tensile stresses generated close to the concave surface of these specimens. It is well known that the applied stresses at the convex and concave region of a TPB specimen should be tensile and compressive, respectively. However, the nature of residual stresses developed in these regions should be just the opposite, producing compressive and tensile stresses, respectively, at these two locations. In view of this rationale, the residual stress data gen-

erated by the ND technique on the TPB specimens appear reasonable and consistent with the established understanding of stress distribution. Some interesting behavior (alternate tensile and compressive residual stresses), however, was observed at some intermediate depths, as shown in Fig. 16 and 17. A similar trend in the measured residual stress data has also been reported by other investigators (Ref 9-12).

An effort was also made to measure the residual stresses in a TPB specimen of EP-823 by the XRD technique. The data, shown in Fig. 18, indicate that the residual stresses were compressive in the vicinity of the apex (convex side), gradually becoming less compressive away from this region. On the contrary, the internal stresses developed at locations close to the concave surface were tensile, gradually becoming less tensile.

3.3 PAS Measurements

The results of the PAS testing on 304L SS and EP-823 at different levels of CR are shown in Fig. 19 and 20, respectively. These data indicate that the magnitude of the T parameter gradually decreased with increasing levels of cold-reduction in both alloys. As indicated earlier, the T parameter is inversely proportional to the induced stresses due to the CR. Thus, the resultant data is consistent in that the lowest value of the T parameter would indicate the maximum residual stresses for both materials.

The residual stresses developed in a welded specimen consisting of 304L SS on both sides were analyzed in terms of the S parameter, determined by the PAS technique, as shown in Fig. 21. An examination of this figure indicates that the magnitude of the S parameter also decreased gradually at locations away from the fusion line, indicating reduced stresses. This observation is also consistent in view of the fact that the S parameter is directly proportional to the residual stresses generated in a welded material. Thus, the highest value of the S parameter would indicate the maximum residual stresses at a location close to the fusion line.

3.4 Comparative Analyses of Residual Stresses

Comparative analyses of residual stresses measured by the RC and ND methods on EP-823, subjected to a cold-reduction of 11.6%, showed a consistent pattern in that the residual stresses were compressive near the surface, and gradually became somewhat tensile at greater depth (Fig. 10 and 14). Similarly, a consistent stress profile was also observed with a welded specimen consisting of HT-9 on both sides, as measured by the RC and ND methods. As illustrated in Fig. 13 and 15, the residual stresses in the vicinity of the fusion line were predominantly tensile in nature. However, as expected, the magnitude of residual stress decreased at locations away from this region. It is a well-accepted fact that the internal stresses

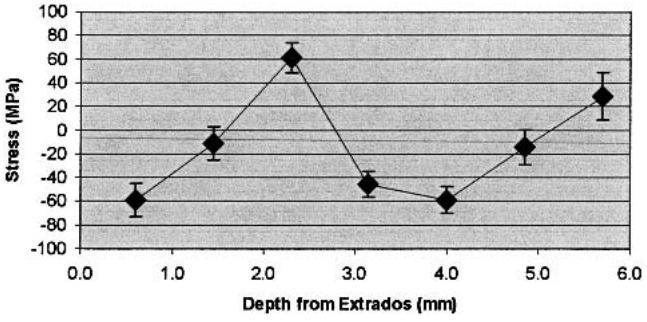

Fig. 16 Residual stress profile for 304L SS TPB specimen (ND method)

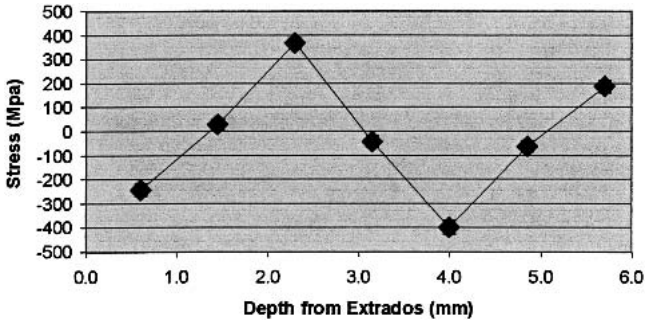

Fig. 17 Residual stress profile for HT-9 TPB specimen (ND method)

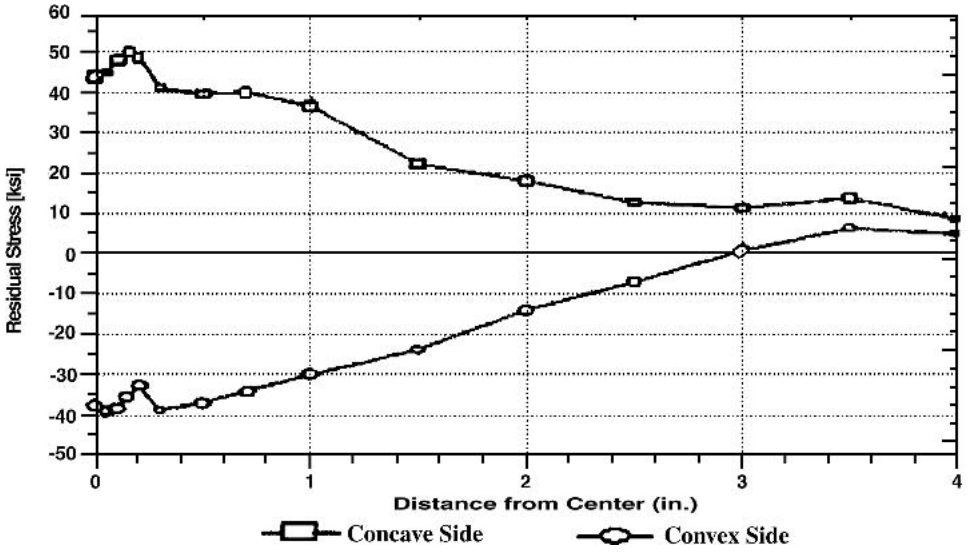

Fig. 18 XRD measurements (longitudinal) on EP-823 TPB specimen

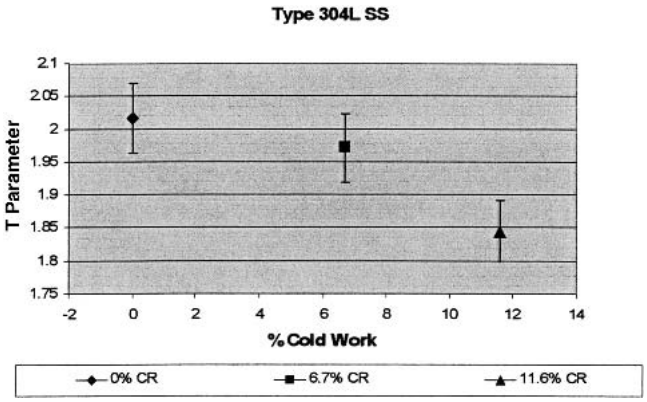

Fig. 19 Effect of percent CW on T parameter (PAS method)

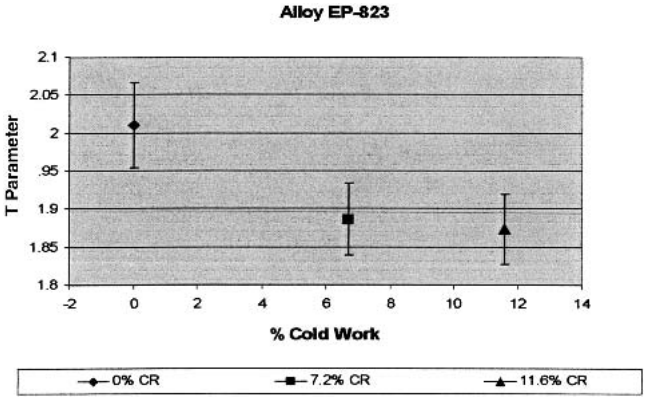

Fig. 20 Effect of percent CW on T parameter (PAS method)

developed at the fusion line of a welded specimen are significantly higher compared to those in the heat-affected-zone and base material. This phenomenon is generally attributed to the different rates of solidification between the weld and the base metals, and the resultant metallurgical microstructural differences between them.

As to the stress profile in the TPB specimens, the resultant data generated by both the ND and XRD techniques showed a similar pattern (Fig. 16, 17, and 18) in that the residual stresses were compressive at the convex surface and tensile at the concave surface. Since a quantitative analysis of the residual stresses developed in the tested specimens could not be performed based on the PAS measurements, no attempt has been made to compare the PAS data to those obtained by the other three techniques.

4. Summary and Conclusions

Residual stress measurements were performed by the RC, ND, XRD, and PAS techniques on three candidate target structural materials including austenitic 304L SS and martensitic EP-823 and HT-9. All four techniques were used to compare residual stresses measured by both destructive and nondestructive techniques. Measurements were performed on CW, TPB, and welded specimens of all three alloys. Comparative analyses of data obtained by different techniques were also performed. The significant conclusions derived from this investigation are summarized below.

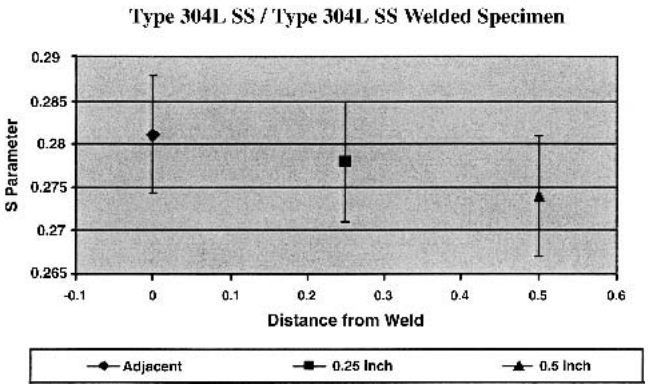

Fig. 21 Effect of weld distance on S parameter (PAS method)

- RC measurements on cold-worked specimens of 304L SS subjected to 6.7% CR revealed tensile residual stresses, whereas compressive residual stresses were observed for EP-823 and HT-9 at a comparable level of CR. This difference in the nature of stress may be attributed to the different metallurgical characteristics resulting from thermal treatments imparted to the austenitic versus the martensitic alloys.
- Residual stress evaluation in cold-reduced (11.6%) specimens of EP-823 by ND similarly showed compressive stresses at the surface followed by tensile stresses at higher depths.
- The PAS data on the cold-worked specimens of EP-823 and 304L SS showed a reduction in the T-parameter value with increased level of cold deformation indicating higher residual stresses.
- Measurements performed by the RC technique on welded specimens of all three alloys with similar material on both sides of the weld revealed tensile residual stresses adjacent to the fusion line. These stresses gradually became compressive at distances away from the fusion line, indicating reduced stresses.
- Similarly, stress measurements by the ND technique on a welded specimen consisting of HT-9 on both sides of the weld showed tensile residual stresses adjacent to the fusion line. Reduced residual stresses were observed at locations away from the fusion line.
- The results of the PAS measurements on a welded specimen of 304L SS showed an enhanced S-parameter value in the vicinity of the fusion line indicating higher stresses.
- The ND measurements on the TPB specimens of HT-9 and 304L SS showed compressive residual stresses at the convex surface and tensile stresses at locations close to the concave surface.
- Comparative analyses of residual stresses determined by different techniques showed consistent patterns. The resultant data indicate that both destructive and nondestructive methods are useful in characterizing residual stresses in structural materials.
- Residual stress measurement by RC and PAS techniques can be accomplished by using portable equipment also.

Acknowledgments

This work was funded through the University of Nevada, Las Vegas, Transmutation Research Program administered by

the Harry Reid Center for environmental studies (United States Department of Energy Grant No. DE-FG04-2001 AL67358).

References

1. S. Keil, Experimental Determination of Residual Stresses with the Ring-Core Method and an Online Measuring System, *Exp. Tech.,* Vol 16 (No. 5), 1992, p 17-24
2. K. Tanaka, Y. Akiniwa, and M. Hayashi, Residual Stress Evaluation by Neutron Diffraction Method, *Mater. Sci. Res. Int.,* Vol 8 (No. 4), Dec 2002, p 165-174
3. R.P. Martukanitz and P.R. Howell, Neutron Diffraction Studies of Welds of Aerospace Aluminum Alloys, in *Nondestructive Evaluation and Material Properties III,* M.E. Hilley, ed., The Minerals, Metals and Materials Society, p 89-95
4. *Residual Stress Measurement by X-Ray Diffraction,* SAE J784a, 2nd ed., Warrendale, PA, 1972
5. I.C. Ismail and J.B. Cohen, *Residual Stress Measurement by Diffraction and Interpretation,* Elsevier Science, Burlington, MA, 1987
6. F.A. Selim, D.P. Wells, J.F. Harmon, J. Kwofie, R. Spaulding, G. Erickson, and T. Roney, Bremssstrahlung-Induced Highly Penetrating Probes for Non-Destructive Assay and Defect Analysis, *Nucl. Instrum. Methods Phys. Res. A,* Vol 495 (No.2), 2002. p 154-160
7. P. Asoka-Kumar, K.G. Lynn, and D.O. Welch, Characterization of Defects in Si and SiO2–Si Using Positrons, *J. Appl. Phys.,* Vol 76 (No. 9), 1994, p 4935-4982
8. P. Hautojarvi and A. Vehanen, *Positrons in Solids,* Springer Verlag, 1979, p 1-20
9. Z. Tan, W.B. Li, and B. Persson, On Analysis and Measurement of Residual Stresses in the Bending of Sheet Steels, *Int. J. Mech. Sci.,* Vol 36 (No. 5), May 1994, p 483-491
10. D. Nowell, S. Tochilin, and D.A. Hills, Measurement of Residual Stresses in Beams and Plates Using the Crack Compliance Technique, *J. Strain Analysis Eng. Design,* Vol 35 (No. 4), Jul 2000, p 277-285
11. M.B. Prime, P. Rangaswamy, M.R. Daymond, and T.G. Abeln, Several Methods Applied to Measuring Residual Stress in a Known Specimen, *Proceedings of the SEM Spring Conference on Experimental and Applied Mechanics,* June 1–3, 1998 (Houston), Society for Experimental Mechanics, 1998, p 497-499
12. M. Hayashi, S. Okido, Y. Morii, N. Minakawa, and J.H Root, Residual Stress Measurements of Structural Components by Neutron Diffraction and Proposal of Measurement Standard, *Mater. Sci. Forum,* Vol 426-432 (No. 5), 2003, p 3969-3974